Two-photon luminescence of gold nanorods: applications to single-particle tracking and spectroscopy

Carozza, S.

Chapter 5

Two-photon excitation spectroscopy of single gold nanorods with multifocal scanning microscope

Gold nanorods are a promising tool for label-free biosensing, with potential applications in cells. The position of their plasmon spectrum shifts in response to changes in the dielectric constant of the environment, caused for example by the interaction with biomolecules. Using single gold nanorods, the shift in the spectrum peak can be used to detect low concentrations of ligands, down to single-molecule level. Two-photon excitation spectra exhibit narrower peaks than one-photon or scattering spectra, and a peak shift can be measured with higher accuracy. We explored the possibility of acquiring two-photon excitation spectra with our two-photon multifocal scanning microscope. When testing different gold nanorods samples, the spectra showed unexpected complexity, apparently unrelated to the sample features. To explain the origin of such spectra, we first verified the two-photon nature of the excitation produced in the sample. Then, we checked for the presence of gold nanorods clusters using electron microscopy images of the sample. Finally, we characterized the response of different elements in the setup to vari-

Two-Photon Excitation Spectroscopy of Single Gold Nanorods for Sensing Applications, S.Carozza, R. Vlieg, J. van Noort. (in preparation partially based on this chapter).

ations in the excitation wavelength. Our results showed that the modulations in excitation power while scanning the wavelength strongly correlate with the shape of the spectra. We pinpointed the elements in the setup responsible for these modulations, hypothesizing that a back-reflection from these elements enters the laser cavity and compromises the two-photon laser output. The experiments reported here were necessary steps for the future successful acquisition of excitation spectra of gold nanorods.

5.1 Introduction

The plasmon resonance of gold nanoparticles (GNPs) depends on the dielectric constant of the surrounding environment (see Chapter 1, Section 1.3.1). Thanks to this feature, GNPs can be used as label-free sensors: molecules binding to the GNP or in its vicinity can be detected by monitoring the shift in the GNP plasmon resonance. This opens up many opportunities in biomedical and chemical research: depending on their functionalization, GNPs can be used to detect molecules such as proteins and DNA [1–3] or chemicals such as heavy metal ions [4]. Interactions between molecules can also be detected, for example antibody-protein interactions, once the GNP sensor is functionalized with the antibody.

Among GNPs, gold nanorods (GNRs) show a notably high sensitivity to dielectric constant changes [3], [5]. The first bio-sensing experiments using GNRs were performed in bulk [1, 6]. The results, however, were partially obscured by the spectral distribution of the particles in the solution. The use of single GNRs improved the detection limit, down to single-molecule level [7].

The sensitivity of a GNR sensor can be maximized by optimizing the GNR size, aspect ratio [8] and functionalization, for example by limiting it to the GNR tips, where the sensitivity is the highest [5]. High resolution in the measurement of the plasmon spectrum is needed to be able to detect small spectral shifts, when the ligand binds to the GNR. Scattering and absorption spectra of GNRs collected by photothermal microscopy [9, 10] and dark-field spectroscopy [7] have been used for sensing experiments. However, due to the non-linear nature of two-photon (TP) excitation, TP spectra of GNRs exhibit a peak which is about 60% narrower than scattering or one-photon excitation spectra [10]. Therefore, we expect TP excitation spectra of GNRs to offer better spectral sensitivity. To our knowledge, plasmon sensing using GNRs was never performed by TP excitation spectroscoy.

When using single GNRs as sensors, multiplexing is advantageous because it provides high throughput. To combine the advantages of TP with wide field imaging, we developed a two-photon multi-focal scanning microscope. The wavelength of our laser source can be tuned automatically and quickly, which allows for acquiring TP excitation spectra with high temporal and spectral resolution. The wide-field excitation makes it possible to acquire images and spectra of all the GNRs in the field of

view in parallel.

In this chapter we investigated the TP excitation spectra of GNRs with different aspect ratios. The position of the peak in a GNR spectrum is proportional to the aspect ratio. The one-photon excitation spectrum of a GNR has a Lorentzian shape [11], so we expected the TP excitation spectrum of a single GNR to follow a squared Lorentzian shape. However, our spectra show multiple, asymmetric peaks. Therefore, we first investigated whether the unexpected spectral features were due to contaminations in the sample or to clustering of GNRs. Then we carried out a detailed characterization of our setup to check for the presence of undesired modulations of the laser intensity in the excitation path that could generate such spectra.

5.2 Materials and methods

Experimental setup

We used a home-made two-photon multifocal scanning microscope to acquire TP images and excitation spectra. A scheme of the setup is shown in Fig. 5.1. A pulsed IR laser (Chameleon Ultra, Coherent) is used for the excitation, with the possibility of automated tuning of the wavelength. A half-wave plate and a polarizing beam splitter (enclosed by a dashed line in Fig. 5.1) are used to tune the light intensity. A quarter wave plate is used to change the light polarization to circular (WPQ05M, Thorlabs). A long-pass filter (LP692, Semrock) blocks the residual visible light in the excitation beam. A diffractive optical element (DOE, custom-made by Holoeye Photonics) is then used to split the laser beam into an array of 25x25 focal spots. The DOE is optimized in the wavelength range 720-800 nm. The array is then scanned by a fast scanning mirror (FSM-300, Newport), to generate a homogenous illumination on the sample, covering an area of about 60 μm x 60 μm. A short-pass filter (SP720, Semrock) is used to filter the residual excitation light. A photodetector (PDA36A, Thorlabs) placed above the sample stage is used to measure the excitation intensity. The same photodetector is used to measure the beam intensity in other positions in the setup, when needed. The setup is described in more details in Chapter 1, Section 1.2.3.

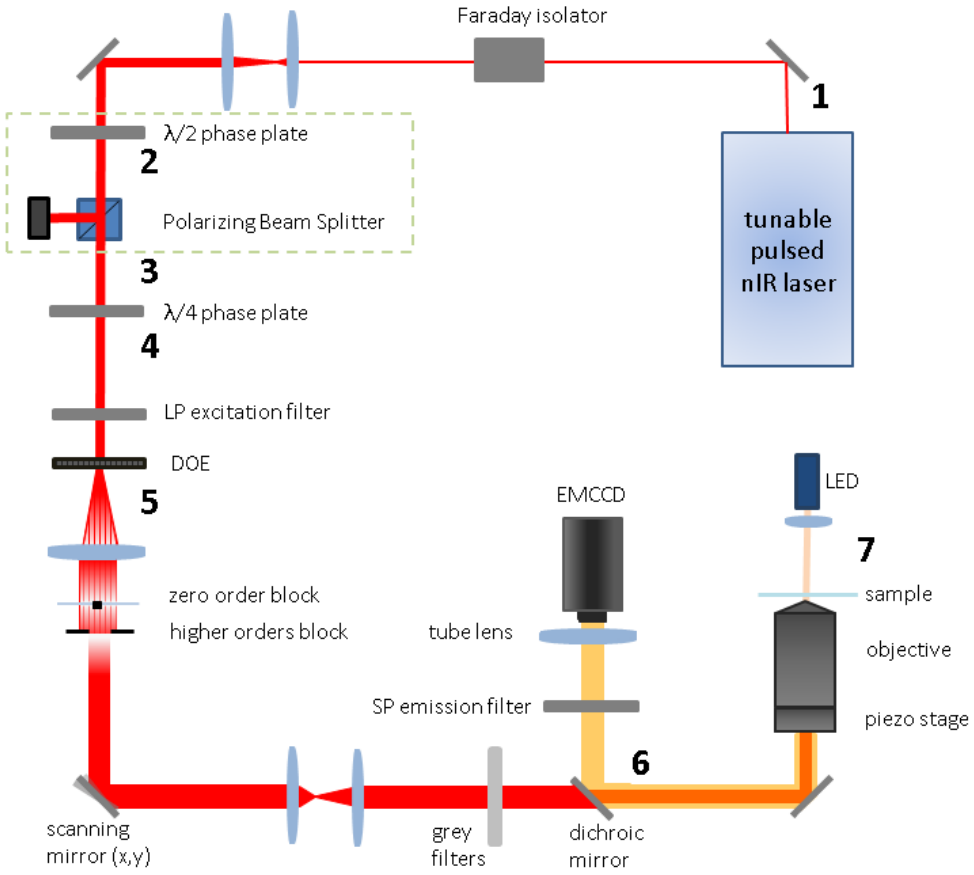

Figure 5.1
Scheme of the two-photon multi-focal scanning setup. Some positions in the setup are marked, and will be referred to in Fig. 5.10.

Sample preparation

Various GNRs samples were used: 780-CTAB, 808-CTAB and 850-CTAB were manufactured by Nanopartz (respectively: A12-25 -780-CTAB, A12-10 -808-CTAB, A12-10 -850-CTAB), 780-PEG and 850-PEG were manufactured by Nanohybrid (78124 and 68630). CTAB (cetyltrimethylammonium bromide) is a surfactant used during seed-mediated synthesis of GNRs. PEG (polyethylene-glycol) is a bio-compatible polymer used to

functionalize GNRs, replacing the CTAB layer.

Samples of GNRs fixed on glass were prepared through the following steps. First, a glass slide was sonicated for 30 minutes in methanol, to remove any pollution from the surface. Then it was sterilized for 30 minutes in a UV-cleaner (Uvo-cleaner, Jelight). To reduce the aggregation between the particles, CTAB-GNRs were diluted in CTAB solution, to adjust the CTAB concentration to 100 μM. The dilution was obtained through a series of (typically 3) dilution and centrifugation steps. The centrifugation was performed at 8000 rpm for 3 minutes. In PEG-GNRs samples, the aggregation was less, thanks to the PEG coating around the particles. After placing a drop of the GNR solution (typically about 30 μl) on the glass slide, the slide was spin-coated in three steps: 200 rpm for 5 seconds, 600 rpm for 15 seconds and 1000 rpm for 60 seconds. The sample was then rinsed gently with demineralized water, dried with a stream of N_2 gas and finally sterilized in the UV-cleaner for 30 minutes. For experiments combining scanning electron microscopy (SEM) or transmission electron microscopy (TEM) and TP imaging, samples were prepared on silicon nitride (SiN) EM grids (home-made as described in [12]), by simply immerging the grid in a GNR solution and drying it with a stream of N_2 gas. To reduce GNRs heating by the laser excitation, a drop of demineralized water was deposited on the slide when performing TP imaging.

TP spectroscopy and imaging with electron microscopes

Spectra were acquired by tuning the laser wavelength while acquiring TP images of the sample. Spectra acquisition and analysis were performed in LabVIEW. The power dependencies were measured by turning a grey filter wheel in the excitation path. UV-Vis spectra were acquired in a UV-Vis spectrophotometer (Cary, Agilent technologies). SEM images were acquired using a NOVA NanoSEM 200 (FEI). TEM images were acquired using a Tecnai 12 TEM (FEI).

5.3 Results and discussion

5.3.1 Excitation spectra of gold nanorods

Fig. 5.2a is a typical image of 780-CTAB GNRs, showing the two-photon signal of all the particles in the field of view. The difference in intensity between GNRs is due to their individual properties: the emission intensity depends both on the particle volume and on the spectral position of the plasmon peak. As we performed experiments with circularly polarized light and we assume the GNRs sticking to the glass slide, the luminescence does not depend on the spatial orientation of the particles. GNRs can form clusters that are brighter than single particles [13]: for this reason, when looking for single GNRs, we ignored very bright and large peaks. The TP excitation spectra of the highlighted particles are displayed in Fig. 5.2b. The different intensities between particles are reflected in the different amplitudes of the peaks in the spectra. We expected spectra with single Lorentzian squared peaks, but in most of the cases the spectra show multiple, asymmetric peaks.

The width of all the peaks is equal or less than 20 nm, as expected for single GNRs according to literature [5]. According to the UV-VIS spectrum of the GNRs sample (Fig. 5.3a), the plasmon peak for this GNR sample is at 750 nm. This position is marked with a blue line in the spectra in Fig. 5.2b: in four cases (GNRs 1, 2, 4, 6) the spectra exhibit a peak in the vicinity.

More spectra from the same sample are shown in Fig. 5.3b. The excitation spectrum and the absorption spectrum of GNRs should overlap, as discussed in Chapter 1, Section 1.3.1. The maximum of the UV-Vis spectrum indicates the position of the plasmon peak, in this case 750 nm (Fig. 5.3a). 10 typical spectra of GNRs in the sample are plotted in Fig. 5.3b. Most of the spectra include multiple peaks, mostly around 760 nm, 790 nm and 830 nm.

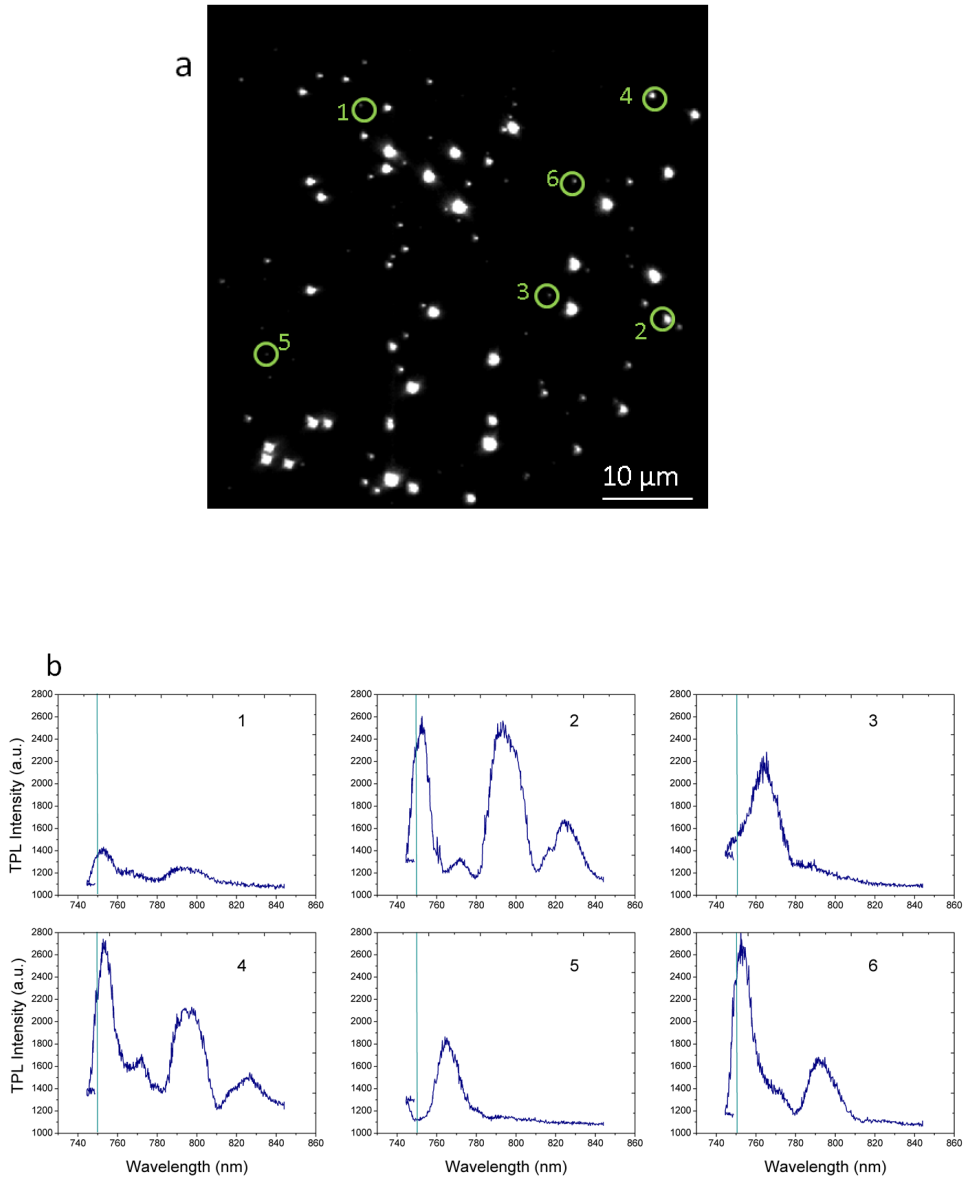

Figure 5.2
A typical TP image and the corresponding excitation spectra of GNRs. a) A TP image of GNRs in a field of view of 60 µm x 60 µm. b) Spectra of the GNRs labeled in a). The expected peak position is marked by a blue line in the spectra. The image in a) was acquired at this wavelength (750 nm).

To check whether the unexpected spectral features are characteristic of the 780-CTAB sample, we acquired spectra of different GNRs samples. Fig. 5.3d shows the results obtained using a sample of 808-CTAB GNRs. The plasmon peak of this sample is at 790 nm, as indicated by the UV-Vis spectrum (Fig. 5.3c). Most of the spectra exhibit multiple peaks (Fig. 5.3d), mostly around 770 nm, 800 nm and 820 nm. Similar results were observed using a sample of 850-CTAB GNRs: while we expected a peak at 820 nm (Fig. 5.3e), most of the peaks are around 750 nm and 770 nm (Fig. 5.3f).

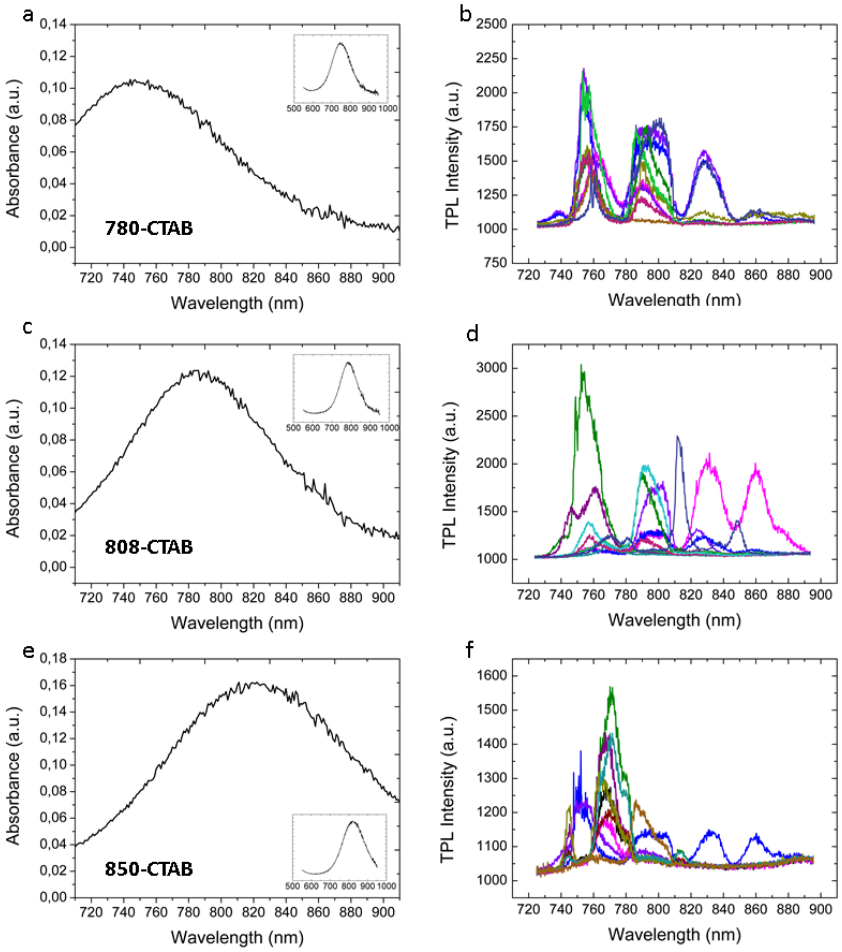

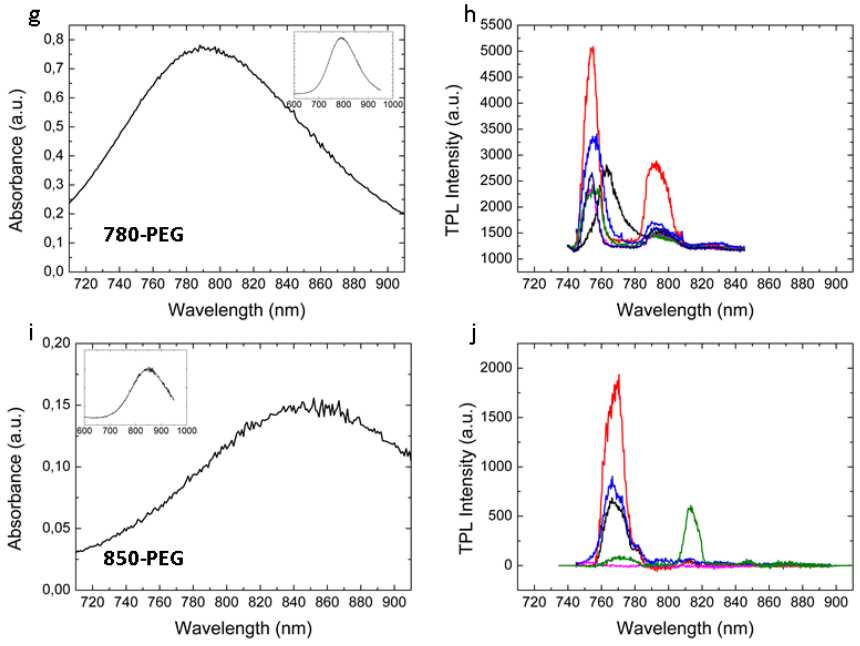

Figure 5.3
Spectroscopy of different GNRs samples: 780-CTAB, 808-CTAB, 850-CTAB, 780-PEG and 850-PEG. a,c,e,g,i) The UV-Vis spectra of the bulk solution indicate the expected peak. The insets show the UV-Vis spectrum from 600 to 1000 nm. b,d,f,h,j) 10 representative TP excitation spectra of GNRs from each sample.

The spectra we obtained do not yield the expected dependence of the plasmon on the aspect ratio of the GNRs. On the contrary, among the three samples a trend in the distribution of the peaks can be noticed: most of the GNRs show three excitation peaks, typically around 760-770 nm, around 800 nm and around 830-860 nm. To find the origin of this discrepancy we tested various hypotheses.

First, we verified whether contaminations in the GNRs sample influenced the spectral features. All three samples were manufactured by Nanopartz and synthetized using CTAB: we therefore analyzed the spectra of two additional samples from a different manufacturer (Nanohybrid), in which the CTAB was replaced with PEG: 780-PEG and 850-PEG. The spectra of these GNRs show similar properties to the previous ones. The UV-Vis spectrum of the 780-PEG GNRs features a peak at

790 nm (Fig. 5.3g), but the single spectra display multiple peaks, including many around 770 nm and 800 nm (Fig. 5.3h). The spectra of 850-PEG GNRs, expected to have a peak at 850 nm (Fig. 5.3i), typically show multiple peaks mostly at 770 and 820 nm (Fig. 5.3j). Hence, we cannot attribute the occurrence of multiple peaks to the presence of CTAB or to the particular production process of a specific batch.

Next, we verified the presence of one-photon emission or scattering light from the GNRs which was not properly blocked by our emission filter. A way to check the nature of the GNR signal is to measure its dependence on the excitation intensity: the emission intensity should follow a quadratic dependence on the excitation intensity. A linear component in the signal will decrease the power dependence of the peak intensity to an exponent closer to 1. We checked the nature of the excitation of GNRs in the 780-CTAB sample, for each wavelength of the spectral peaks: an example is shown in Fig. 5.4. All the three peaks in the spectrum (Fig. 5.4a) exhibit a quadratic dependence on the excitation intensity (Fig. 5.4b, c, d). Moreover, adding an extra emission filter did not remove any of the peaks in the spectra (data not shown). From these results we can exclude the presence of a one-photon excitation or scattering component in the peaks of the spectrum, which could obscure the two-photon luminescence.

We then checked whether the peaks in the spectra are also present in the background signal. The background spectrum of the TP image in Fig. 5.2 is plotted in Fig. 5.5a, together with the spectrum of the GNR number 5 before and after subtraction of the background. The background of our TP images features a weak dependence on the excitation wavelength. The wavelength dependence of the background hardly affects the shape of the spectra. In the rest of this chapter, the background is subtracted from the spectra.

Because of the sharp plasmon peak, we expected little influence of the excitation power profile as the wavelength is scanned. The more so, as the output spectrum of the laser (as provided by Coherent), only features a gradual change over its wavelength range. When we measured the excitation power by putting a photodiode above the sample however, the spectrum showed a noticeable dependence on the excitation wavelength, with peaks at 765 nm, 796 nm and 825 nm (Fig. 5.5b), i.e. at positions comparable to the peaks in the spectra. To account for the differences

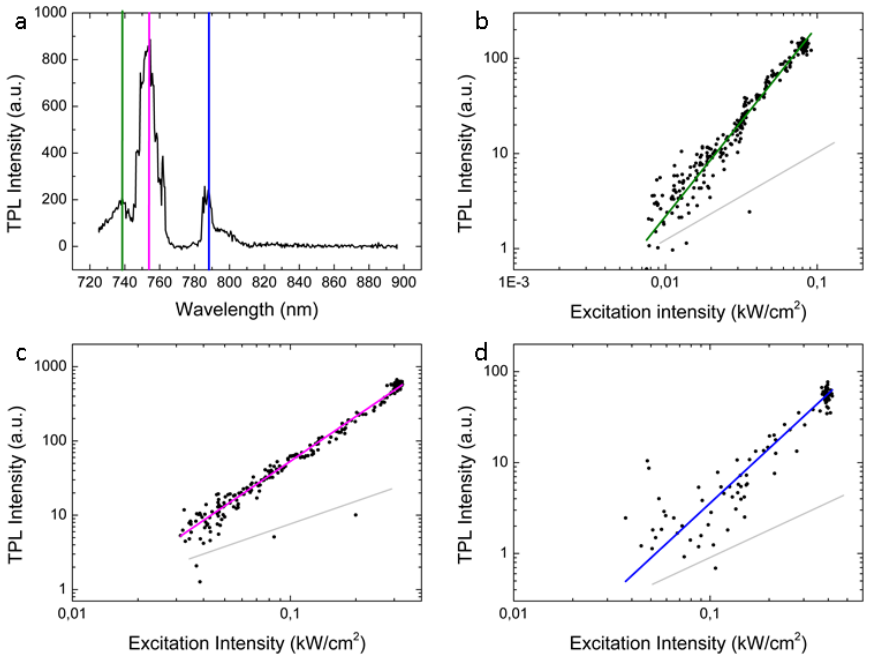

Figure 5.4
Quadratic dependence of the peaks in a GNR spectrum. b-d) The power dependence of all three peaks in a GNR spectrum (a) are analyzed to check the nature of the excitation process. The power dependences have been acquired at the wavelengths highlighted in a). In each case, the colored line indicates the fit with slope 2. For comparison, a line with slope 1 is also depicted in grey in every image.

in excitation power, the emission signal was corrected according to:

$$I_{corrected}(\lambda) = I(\lambda)/(I_{excitation}(\lambda))^2 \tag{5.1}$$

which takes into consideration the non-linear nature of excitation. Nevertheless, correcting the spectra changes their shape only slightly: in Fig. 5.5b and Fig. 5.5c the spectra of GNRs 5 and 4 from Fig. 5.2 are shown, before and after the correction. The three peaks remain, though the intensity is redistributed among the peaks.

The fact that the peaks in the excitation profile partially overlap with the peaks in the GNRs spectra and that these peaks cannot be eliminated by dividing the GNR spectra by the square of the excitation profile suggests a more severe influence of the laser modulation.

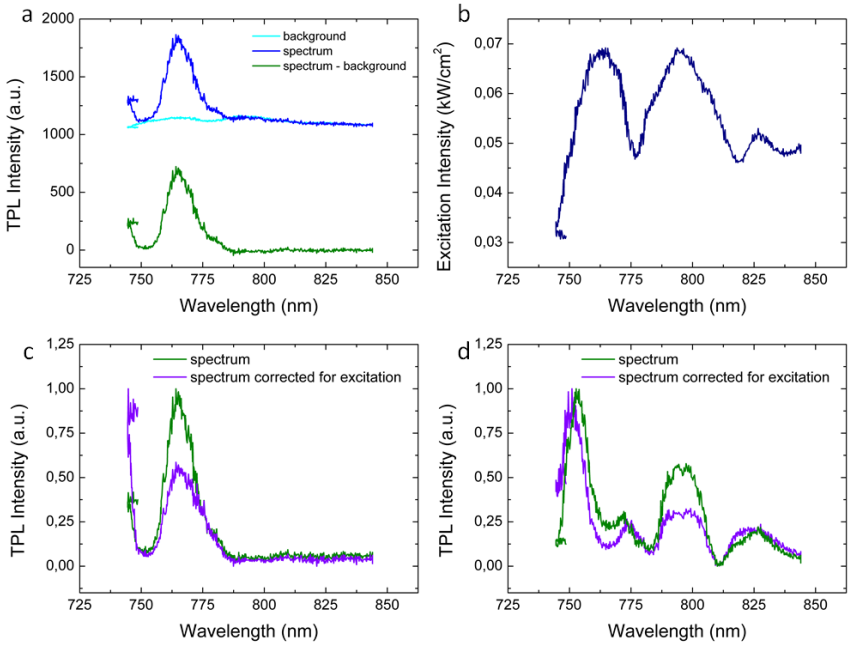

Figure 5.5

The influence of background and excitation intensity profile on GNR spectra. a) Dependence of the background signal on the wavelenght and its influence on the spectrum of GNR 5 from Fig. 5.2. The background spectrum (light blue curve) was measured in a part of the sample without GNRs. The original GNR spectrum (blue curve) and the result of the subtraction by the background (green curve) are shown. b) Dependence of the excitation intensity on the wavelength. The excitation profile was measured with a photodetector placed above the sample stage. c,d) Two examples of spectra corrected by the excitation intensity. The spectra correspond to GNR 5 and GNR 4 in Fig. 5.2).

5.3.2 Characterization of gold nanorod samples with electron microscopy

As opposed to single particles, the excitation of GNRs clusters can cause an unpredictable spectral response that depends on the number of particles in the cluster and their spatial arrangement. It was reported that GNRs clusters present multiple and asymmetric spectra [14], similarly to what we observe. A way to directly check for the presence of clusters is to look at the GNRs with an electron microscope. We acquired SEM images of a 780-CTAB GNR sample. We observed a variety of particles configurations, as shown in Fig. 5.6. We zoomed in on 37 particles in different areas of the sample. Half of them were single: 15 GNRs and 3 spheres. There were 19 clusters, among which 6 doublets and 3 made by single GNRs, not connected, but too close to be resolved by optical microscopy. Therefore, even though there are many clusters, the number of single GNRs is large enough to expect some single GNRs spectra.

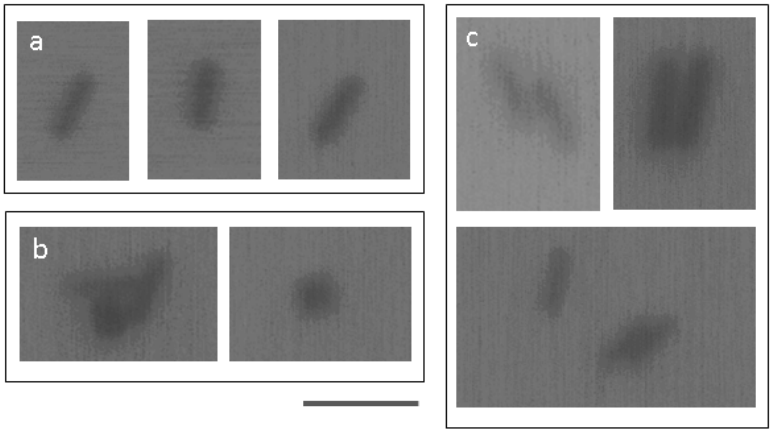

Figure 5.6
SEM images reveal the composition of a GNR sample. A sample of 780-CTAB GNRs was prepared on a TEM grid. Examples of configurations are shown: a) single GNRs, b) clusters and single spheres, c) GNRs doublets. The size bar corresponds to 50 nm.

The only definitive way to check whether our spectra relate to single GNRs or clusters was to correlate electron microscope images with spectra of the same particles. For this experiment we used a TEM. We first acquired a TP image, together with the excitation spectra of all the GNRs in a marked area in the sample. Then we acquired TEM images of the same area, and we overlapped them to the TP images, as in Fig. 5.7a. The overlapped TEM and TP image of 2 single GNRs are shown in Fig. 5.7b and Fig. 5.7d; the overlapped images of 2 clusters are shown in Fig. 5.7f and Fig. 5.7h. The excitation spectra (Fig. 5.7c,e,g,i) are reported next to these images. No clear difference was found between the spectra of single GNRs and those of clusters, neither in the number of peaks nor in their shape.

Unexpectedly, the most symmetric spectrum (Fig. 5.7l) belongs to a cluster. The spectrum of the second cluster (Fig. 5.7h,i j) is not distinguishable from the spectra of the single particles.

In conclusion, we observed irregular spectra both for single GNRs and clusters. Therefore, such spectra cannot be explained by the presence of GNRs clusters.

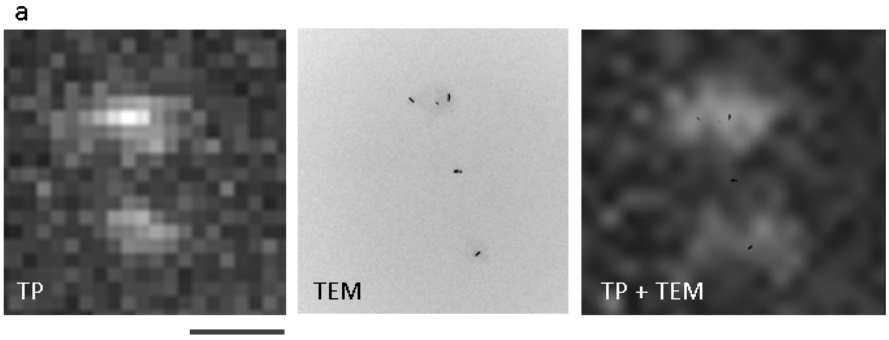

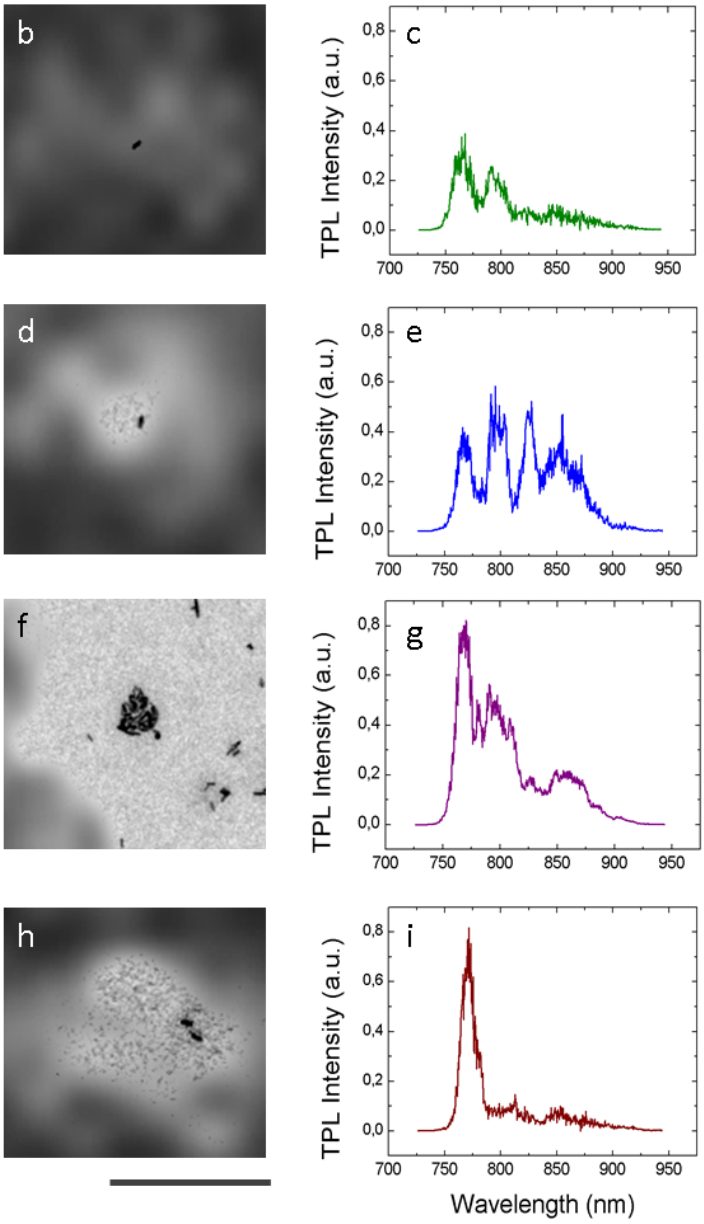

Figure 5.7
Correlation between TEM images, TP images and spectra. TEM and TP images of the same GNRs from a 780-CTAB sample were acquired. a) Overlap of the TP and TEM images of the same area in the sample. (b-d) Overlap of TEM and TP images of two single particles and (f,h) two clusters, with their excitation spectra in c,e,g,i). The scale bar corresponds to 1 μm.

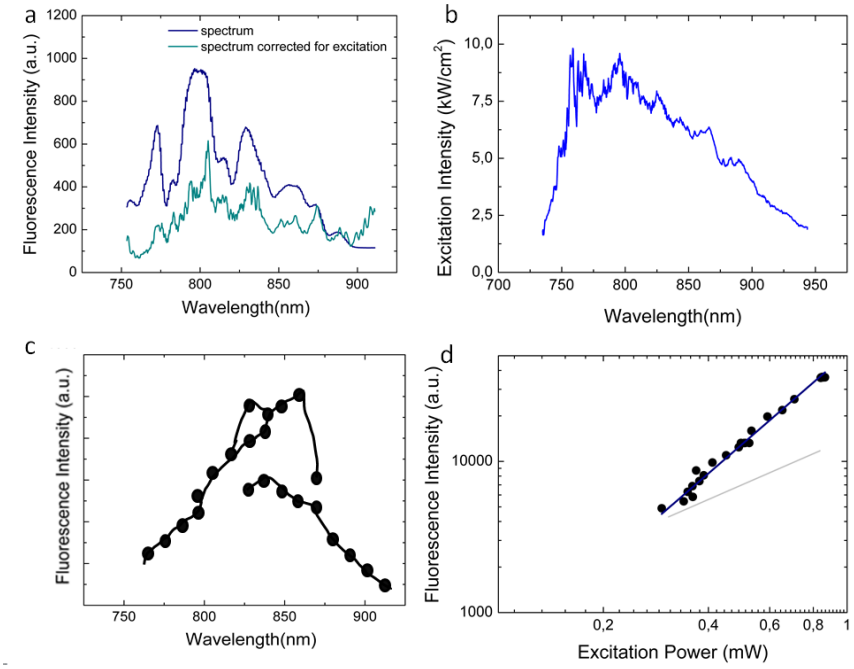

Figure 5.8
Experiments with Rhodamine-B solution. a) TP excitation spectrum of Rhodamine-B in methanol acquired in our setup, before (blue line) and after the correction (cyan line) by the excitation intensity. b) Excitation intensity profile. The expected TP excitation spectrum of Rhodamine-B in methanol follows the excitation cross-section spectrum shown in c, reconstructed from the original figure from [15]. d) Quadratic power dependence of Rhodamine-B in methanol.

5.3.3 Excitation spectrum of Rhodamine-B

As a last check to exclude the sample quality as source of irregularity in the spectra, we measured the spectrum of a homogenous dye solution. The TP excitation spectrum of Rhodamine-B is shown in Fig. 5.8a (blue line). As in the case of GNRs, we obtained multiple peaks that could not be removed by correcting the spectrum by the excitation intensity profile (plotted in Fig. 5.8b). The corrected spectrum is shown in Fig. 5.8a (cyan line). The TP excitation spectrum of Rhodamine-B reported in literature (Fig. 5.8c, a reconstructed detail from the original image from [15],) exhibits also multiple peaks, but in different positions than

the peaks we obtained. The positions of the peaks in our spectrum are comparable to the ones in GNRs spectra: an indication that the spectra hardly reflect the properties of the sample, and is therefore likely to be due only to signal modulations originating in the setup. The quadratic power dependence of TP fluorescence was verified (Fig. 5.8d).

5.3.4 Characterization of the setup

A multi-focus scanning system has not been used before to perform excitation spectroscopy. We therefore verified how scanning the wavelength affects the wide-field illumination. The pattern of focal spots created by the DOE features slightly different sizes and positions at different wavelengths. Fig. 5.9a shows the array of spots at 740, 780 and 890 nm, as measured by imaging the reflected beam on a glass slide. For this experiment, we removed the emission filter. The pattern increases in size when changing the wavelength from 740 nm to 890 nm, and it has a maximum intensity at around 780 nm. Fig. 5.9b shows the intensity profile along the marked line in every image. A misalignement in the x-y plane causes the appearance of the zero order diffraction peak in the center of the pattern (see last figure), that is normally filtered in the excitation path by a zero-order block.

To obtain a wide and homogeneous illumination we scan the focal spot pattern using a spiral function, as described in Chapter 1, Section 1.2.3. The effect of the spiral scanning on the excitation pattern at different wavelengths is shown in Fig. 5.9c. The widening of the pattern at larger wavelengths causes the scanned spirals to be smaller than the distance between the peaks of the diffraction pattern. To check whether this compromises the homogeneity of the excitation, we measured the intensity profile of the pattern along the marked line at different wavelengths (Fig. 5.9d). The homogeneity of the intensity profile changes, but not dramatically, and an adjustment of the amplitude of the spirals can solve this issue.

We measured the distance between focal spots in the plots of Fig. 5.9b, obtaining a value of 3.6 μm at 890 nm, about 0.9 μm larger than at 740 nm (Table S1). We also measured the width of the focal spots: the difference is 0.2 μm between the pattern at 740 and 890 nm. The spiral amplitude we use for our experiment is 2.4 μm. However, changing the amplitude of the scanning spirals does not influence the number, quality

and position of the peaks in a GNR spectrum (Fig. S1).

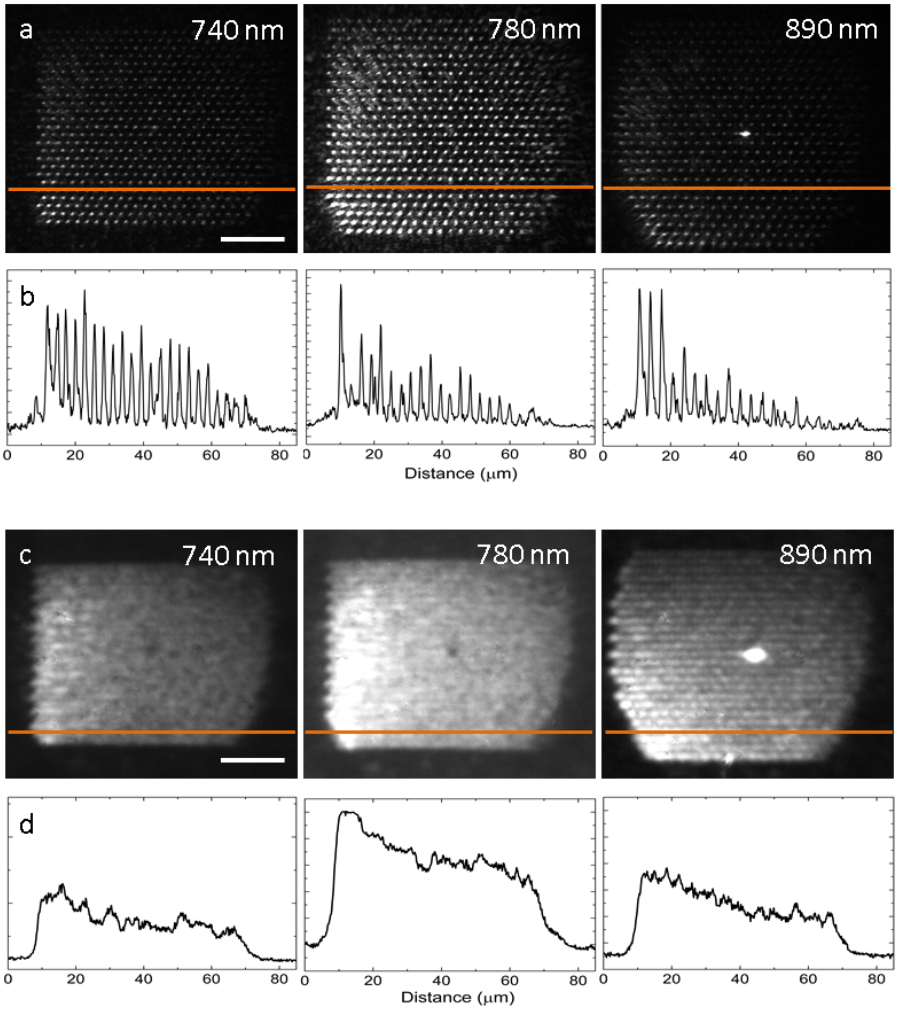

Figure 5.9

Size and homogeneity of the excitation pattern at different wavelengths. a) The array of focal spots generated at different wavelengths. b) Plot of the intensity profile along the marked line in each image. c) The effect of wavelength on the homogeneous pattern created by spiral scanning. d) Intensity profile along the marked line in each image is plotted. In both a and c, a decrease in intensity from right to left can be noticed, due to a slightly tilted position of the DOE. The scale bars are 10 μm.

When tuning the wavelength, the excitation pattern also moves slightly in the z direction. However, the size of this shift is within the size of our focal spot (around 1 μm in z) and therefore we do not expect it to affect the excitation of the sample. The spectra of the same GNR acquired at different z positions, shown in Fig. S1b, confirm this. Therefore, the multifocal system and the spiral scanning are not responsible for the peaks we observe in the spectra.

To exclude the DOE as one of the causes of artefacts in the spectrum, we tested two different configurations to obtain a wide-field excitation. An alternative method to obtain a pattern of focal spots is to use a micro lens array (MLA) instead than a DOE. However, the spectra obtained with this method showed similar features as obtained with the DOE (Fig. S2). Also using the setup in total internal reflection mode yielded the same results (data not shown).

We finally analyzed how the intensity of the laser light is affected by scanning the wavelength at each component of the setup. In Fig. 5.1 we labeled various locations in the setup. Their corresponding spectra are shown in Fig. 5.10. The spectrum at the laser output (1) shows a quite homogeneous bell-shape, centered at 824 nm. This profile is unmodified till after the polarizing beam splitter (3): here three peaks appear in the profile, around 795, 825 and 865 nm. The peak at 825 nm becomes more pronounced after the half-wave plate (4), while modulations appear in the other two peaks. A spectrum with three main peaks at 765, 795 and 825 nm is maintained throughout the setup till after the objective (7), while the peak at 865 nm undergoes some variations. These peaks coincide with the ones we see in most of our spectra. Thus, the polarizing beam splitter and the quarter-wave plate appeared to be responsible for the modulations in the laser intensity.

Later experiments carried out in our group showed a major improvement in the spectra after removing the polarizing beam splitter and the quarter-wave plate. Unfortunately, these experiments were performed after finishing the experimental work presented in this thesis.

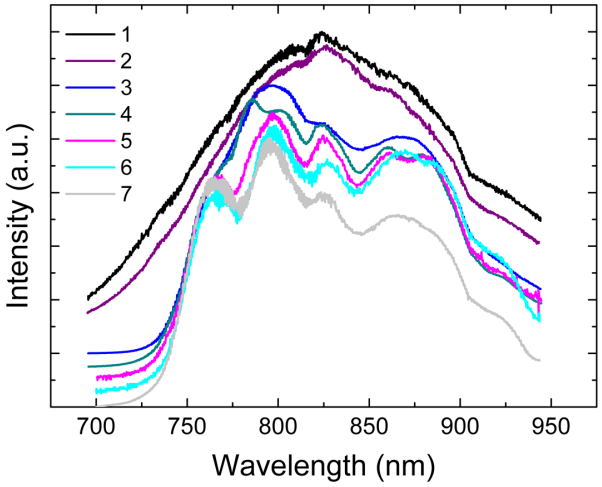

Figure 5.10
Excitation profile transmitted by some elements in the setup. The curves refer to the elements marked with numbers in the setup scheme of Fig. 5.1.

5.4 Conclusion

Using a multifocus scanning TP microscope, we acquired GNRs spectra that exhibited multiple unexpected, asymmetric peaks. These peaks were found for GNRs with different aspect ratios, and therefore do not represent the characteristics of the GNRs in the sample.

Multiple and asymmetric peaks in GNRs spectra were previously observed as a consequence of Fano-resonance, a result of the interference between resonances modes in the particle [16]: however the Fano spectra had different shape than the spectra we observe. Furthermore, this phenomenon was observed only for long GNRs deposited on substrates with a large dielectric constant, and not on glass [17]: Fano resonance therefore cannot explain our spectra.

We tested several other hypotheses on the origin of these peaks in the excitation spectra:

1. signal from a contamination present in the GNR samples;
2. one-photon luminescence or scattering signal from the GNRs;
3. signal emitted by clusters of GNRs;

4. artifacts caused by one or more elements in the setup.

We tested the first hypothesis by performing experiments on samples of PEG-GNRs produced by a different manufacturer, but the spectra exhibited the same features.

We observed modulations in the excitation intensity spectrum that could be amplified by the non-linear character of the TP excitation. However, corrections by dividing the GNR spectra by the square of the excitation intensity was not enough to yield a single, sharp spectrum. This correction could fail if the emission resulted from a mixture of one-photon and two-photon excitation processes. Nevertheless, all peaks featured a quadratic dependence on excitation power: the two photon signal was therefore not mixed with a linear component. The excitation profile we used for our correction was measured above the sample and it could be an inaccurate approximation of the actual excitation profile in the sample. Thermal reshaping of the GNRs could also induce an unstable, broadened spectrum. However, the similarities in the spectra obtained from GNRs with different aspect ratio and the partial overlap of the spectra with the excitation profile are likely to exclude these two hypotheses. The presence of clusters as the reason for the observed spectra was excluded by correlating TP spectra with TEM images of the same GNRs.

The spectrum of Rhodamine-B solution showed spectral features similar to those of GNRs, confirming that these features can not to be attributed to the sample but they originate in the setup.

We therefore performed a detailed characterization of our setup when scanning the wavelength. We first investigated how the wavelength scanning affects the spatial homogeneity of the illumination. Changing the wavelength slightly affected the size of the excitation pattern, but this did not influence the shape of the spectra.

We then analyzed how the spectral excitation intensity modulation developed through the optical path. We checked the spectrum at every component in the excitation path and identified the components where first the peaks appear: the polarizing beam splitter used to control the laser intensity and the quarter-wave plate used to change the light polarization. In our group it was later shown that removing these elements eliminated the unexpected peaks in the GNRs spectra.

The reason why removing the elements responsible for the modula-

tions improved the spectra but correcting the spectra for the square of the modulation profile did not, is not straightforward. We hypothesize that a backreflection, originating from these elements for some specific wavelengths, entered the laser cavity and compromised the quality of the laser beam. We checked the beam intensity at the laser output, but not the pulse width nor the mode and how these parameters were influenced by the presence of the polarization optics. During future spectral measurements these parameters should be accurately monitored. We used a broadband Faraday isolator to filter the backreflections, but we could not find details on its efficiency within the spectral range we use. Moreover, the efficiency of the isolator depends on the polarization of the beam, hence the reflected light coming from the polarizing opticsc may not be blocked properly. The polarizing beam splitter and the half-wave plate were removed from the setup, but they could be useful in the future to automatically tune the excitation intensity and to acquire circular polarized spectra of the GNRs. The proposed checks should then be carried out, to be able to eliminate the modulations produced by these elements.

A laser intensity modulator might be used to reduce the modulations introduced by the optics. Also an analysis of the transmission of the elements along the emission path may be carried out, to verify whether additional modulations are introduced along the emission path. This check can be done placing a white light source instead of the laser and analyzing the transmissivity of each element in the path. Alternatively, each element might be taken out of the setup and into a spectrometer for proper characterization.

In conclusion, the experiments we presented here, including EM characterization of the GNRs sample to check for single particles and a detailed analysis of the setup response to wavelength scanning, were a necessary step for successfull spectroscopy experiments. We localized the elements in the setup where the unexpected peaks in the spectra originated, and removing them brought major improvements. When new experiments show sharp and narrow peaks of single GNRs, it will be possible to explore the potential that TP excitation spectra offer for biosensing applications.

5.5 Supplementary figures

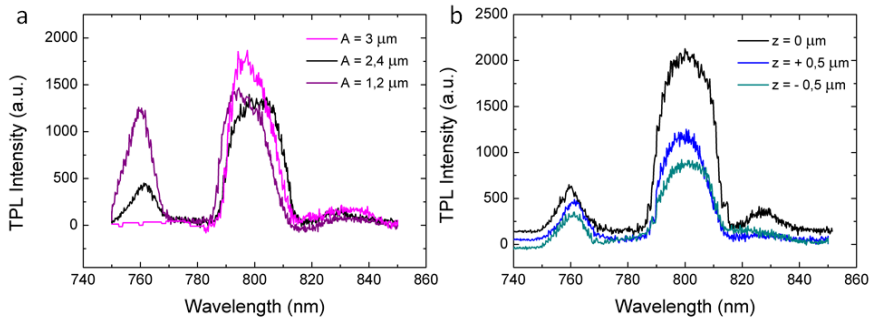

Figure S1
a) TP excitation spectra of a GNR acquired with different amplitude of the scanning spirals. The number and shape of the peaks in the spectra is not influenced by the scanning amplitude. The initial flat part in the curve with A=0.3 µm is due to a laser problem, not to the amplitude of the spirals. In b) the spectra of the same GNRs are acquired at different heights: in focus (z = 0 µm), and 0.5 µm above or below the focus.

Wavelength (nm)	Distance between spots (µm)	Spot width (µm)
740	2.7 ± 0.1	0.7 ± 0.1
780	3.1 ± 0.03	0.7 ± 0.1
890	3.6 ± 0.4	0.9 ± 0.02

Table S1
Distance between spots and spots widths measured along the lines in Fig. 5.9.

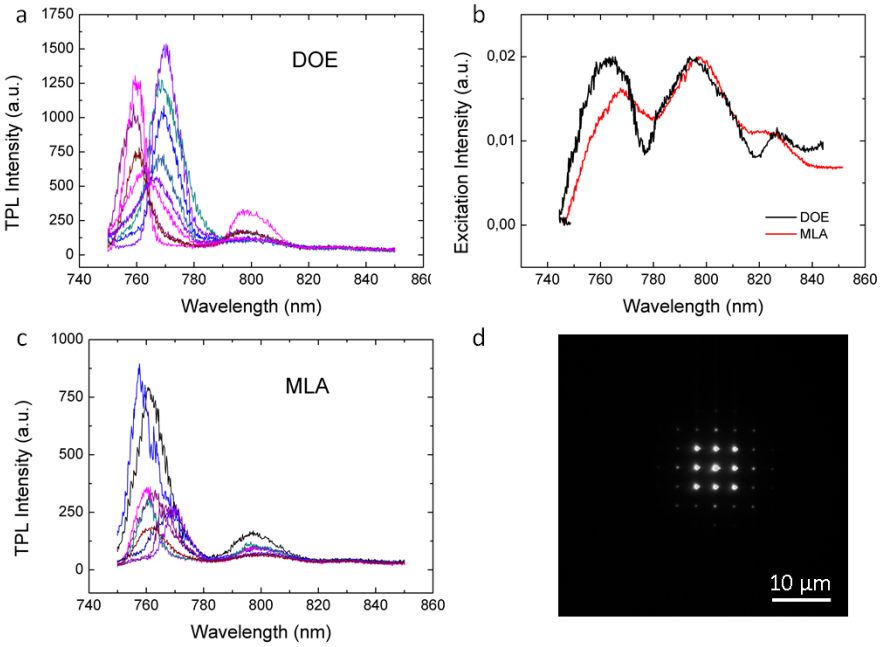

Figure S2

Difference between spectra acquired with a DOE and with a microlens array (MLA). Spectra of 780-CTAB samples were measured using a) a DOE and c) a MLA for the excitation. In the two cases, the GNRs are not the same particles. b) Comparison of the excitation intensity profiles produced by the DOE and by the MLA, as measured above the sample. d) Pattern of excitation produced by the MLA.

Bibliography

[1] Cheng-Dah Chen et al. "Sensing capability of the localized surface plasmon resonance of gold nanorods." In: *Biosensors & bioelectronics* 22.6 (Jan. 2007), pp. 926–32. ISSN: 0956-5663.

[2] Nguyen Thi Kim Thanh and Zeev Rosenzweig. "Development of an Aggregation-Based Immunoassay for Anti-Protein A Using Gold Nanoparticles". In: *Analytical Chemistry* 74.7 (Apr. 2002), pp. 1624–1628. ISSN: 0003-2700.

[3] Shuwen Zeng et al. "A Review on Functionalized Gold Nanoparticles for Biosensing Applications". en. In: *Plasmonics* 6.3 (Apr. 2011), pp. 491–506. ISSN: 1557-1955.

[4] Gopala Krishna Darbha et al. "Selective detection of mercury (II) ion using nonlinear optical properties of gold nanoparticles." In: *Journal of the American Chemical Society* 130.25 (June 2008), pp. 8038–43. ISSN: 1520-5126.

[5] P Zijlstra and M Orrit. "Single metal nanoparticles: optical detection, spectroscopy and applications". en. In: *Reports on Progress in Physics* 74.10 (Oct. 2011), p. 106401. ISSN: 0034-4885.

[6] Nidhi Nath and Ashutosh Chilkoti. "A Colorimetric Gold Nanoparticle Sensor To Interrogate Biomolecular Interactions in Real Time on a Surface". In: *Analytical Chemistry* 74.3 (Feb. 2002), pp. 504–509. ISSN: 0003-2700.

[7] Irene Ament et al. "Single unlabeled protein detection on individual plasmonic nanoparticles." In: *Nano letters* 12.2 (Feb. 2012), pp. 1092–5. ISSN: 1530-6992.

[8] Kyeong-Seok Lee and Mostafa A El-Sayed. "Gold and silver nanoparticles in sensing and imaging: sensitivity of plasmon response to size, shape, and metal composition." In: *The journal of physical chemistry. B* 110.39 (Oct. 2006), pp. 19220–5. ISSN: 1520-6106.

[9] Michael A Beuwer, Menno W J Prins, and Peter Zijlstra. "Stochastic Protein Interactions Monitored by Hundreds of Single-Molecule Plasmonic Biosensors." In: *Nano letters* 15.5 (Apr. 2015), pp. 3507–3511. ISSN: 1530-6992.

[10] Peter Zijlstra, James W M Chon, and Min Gu. "Five-dimensional optical recording mediated by surface plasmons in gold nanorods." In: *Nature* 459.7245 (May 2009), pp. 410–3. ISSN: 1476-4687.

[11] Carolina Novo et al. "Contributions from radiation damping and surface scattering to the linewidth of the longitudinal plasmon band of gold nanorods: a single particle study". en. In: *Physical Chemistry Chemical Physics* 8.30 (July 2006), p. 3540. ISSN: 1463-9076.

[12] Roman I. Koning, Gert T. Oostergetel, and Alain Brisson. "Preparation of flat carbon support films". In: *Ultramicroscopy* 94.3-4 (Apr. 2003), pp. 183–191. ISSN: 03043991.

[13] Babak Nikoobakht and Mostafa A. El-Sayed. "Preparation and Growth Mechanism of Gold Nanorods (NRs) Using Seed-Mediated Growth Method". In: *Chemistry of Materials* 15.10 (May 2003), pp. 1957–1962. ISSN: 0897-4756.

[14] Alison M Funston et al. "Plasmon coupling of gold nanorods at short distances and in different geometries." In: *Nano letters* 9.4 (Apr. 2009), pp. 1651–8. ISSN: 1530-6992.

[15] Chris Xu and Watt W. Webb. "Measurement of two-photon excitation cross sections of molecular fluorophores with data from 690 to 1050 nm". In: *Journal of the Optical Society of America B* 13.3 (Mar. 1996), p. 481. ISSN: 0740-3224.

[16] F López-Tejeira et al. "Fano-like interference of plasmon resonances at a single rod-shaped nanoantenna". en. In: *New Journal of Physics* 14.2 (Feb. 2012), p. 023035. ISSN: 1367-2630.

[17] Huanjun Chen et al. "Observation of the Fano resonance in gold nanorods supported on high-dielectric-constant substrates." In: *ACS nano* 5.8 (Aug. 2011), pp. 6754–63. ISSN: 1936-086X.